Solar-like oscillating red-giants in eclipsing binaries and their importance in astrophysics

M. Yıldız★, S. Örtel and T. Çakır Alsaç
Department of Astronomy and Space Sciences, Faculty of Science, Ege University, 35100 İzmir, Turkey.

Accepted XXX. Received YYY; in original form ZZZ

ABSTRACT

The study of solar-like oscillating red giants (RGs) in eclipsing binaries (EBs) provides a unique opportunity to advance stellar astrophysics by synergising dynamical mass and radius measurements with asteroseismic constraints. EBs provide precise fundamental parameters (e.g., mass, radius and luminosity) independent of distance, while solar-like oscillations act as probes of stellar interiors and tools for determining asteroseismic scaling relations to obtain stellar mass and radius. By applying two different methods, we construct interior models for the components of 11 EBs and find very exact solutions for seven of them. The ages and chemical compositions found by the two methods agree with each other. Our results offer interesting findings about the chemical evolution in a part of the galactic disk and the mass gain and loss of the RG components. Moreover, using the values we obtained for two of these oscillating stars (Tek Ayak (KIC 8410637) and KIC 9970396) instead of the solar values in the scaling relations makes the orbital analysis results very compatible with the results obtained using the scaling relations without any correction.

Key words: stars: eclipsing binaries, stars: oscillation, stars: interior, stars: evolution

1 INTRODUCTION

Eclipsing binaries (EB) in general, and more recently solar-like oscillating (SLO) stars in great, are of particular importance in obtaining fundamental stellar parameters and testing the theory of stellar evolution. EBs with SLO components are invaluable in this respect. Such EB stars are among the Kepler targets (Frandsen et al. 2013; Gaulme et al. 2016; Beck et al. 2024; Grossmann et al. 2025). The red giant (RG) component of some of these EBs exhibits solar-like oscillations. These stars should be considered very special laboratories for testing the theory of stellar evolution. Considering that most of the stars detected by the Transiting Exoplanet Survey Satellite (*TESS*, Sullivan et al. 2015) and *Kepler* (Borucki et al. 2010) missions are RGs, the importance of these SLO EBs becomes even clearer.

Joint binary star and asteroseismological modelling improves stellar age determination. In this regard, comprehensive studies have been conducted recently by analysing high-quality data (Frandsen et al. 2013; Gaulme et al. 2016; Beck et al. 2024; Grossmann et al. 2025). To leverage this advantageous situation, the analyses must shed light on the mass loss and gain in the binaries.

The mass (M), radius (R), effective temperature ($T_{\rm eff}$) and metallicity ([Fe/H]) parameters of the components have been determined from observational spectral and photometric data (Gaulme et al. 2016). It is important to determine the ages and chemical compositions of the binary stars well for many reasons. For example, this information can shed light on the chemical evolution of the Milky Way. We can construct internal structure models of the components using common age and chemical composition constraints. These stars are very important in two respects. First, because the evolutionary properties of the components are very different from each other (see Rowan et al. 2024), we can determine the properties of the system uniquely. These systems are perhaps the most suitable for a unique solution. Second, we can use one of these stars as a unit star for the scaling relations between the asteroseismic and non-asteroseismic parameters of these stars. Thus, we use the values for this star instead of the solar values. The selected unit star can be used to calculate the fundamental parameters of stars with high-quality asteroseismic data (e.g., RGs in APOKASC-2, Pinsonneault et al. 2018). For example, it is better to use an RG as the unit star instead of the Sun in scaling relationships (see Figure 10).

The observational basic parameters of the 11 EB stars were compiled from the literature (Frandsen et al. 2013; Rawls et al. 2016; Gaulme et al. 2016; Brogaard et al. 2018; Themeßl et al. 2018; Brogaard et al. 2022). The primary stars (oscillating components) are all located in the region of the RGs. These stars may be ascending stars in the RG branch or red clump (RC) stars burning helium in their core (see Section 4). Most of the secondary components are around the main sequence (MS). One of the secondary components is about to reach the RG branch (KIC 4054905 B), while another appears to be slightly more evolved (KIC 9246715 B).

The mass−metallicity (MZ) diagram is particularly important in determining the structural and evolutionary status of RG stars, particularly for mass-gaining and mass-losing processes. Most RGs in APOKASC-2 are populated in a triangle in the MZ diagram (Yıldız 2023). The outsiders are potential stars that have gained or lost mass. The position of the 11 SLO components in the diagram should be

★ E-mail: mutlu.yildiz@ege.edu.tr

considered when constructing the interior models of these stars (see Figs. 2, 7, and 8).

Using the MESA (Paxton et al. 2011, 2013, 2015, 2018, 2019; Jermyn et al. 2023) code, we constructed non-rotating interior models of the primary and secondary components and sought to align these models to the observed radii and luminosity. It is widely accepted that the component stars of a binary system have the same age and chemical composition. We can take the initial metallicity (Z_0) as the surface metallicity (Z_s), calculated from the observed metallicity of the binary or its RG component. Since the secondary star is around the MS, the initial and surface chemical compositions differ significantly because of diffusion, depending on the age and depth of the convective zone. The surface chemical composition of the RG component is extremely close to the initial chemical composition because of the effect of the first dredge-up. The initial helium abundance of the system (Y_0) can be computed from either calibration or from Z_0, assuming that the chemical enrichment in the galactic disk proceeds as $Y_0 = Y_p + cZ_0$, where Y_p is the primordial helium abundance (Planck Collaboration et al. 2020) and c is the factor to be tested. In the evolutionary grids, we chose $c = 2$.

The rest of this paper is organised as follows. Section 2 presents and discusses the observational data of the binaries. The models are described in Section 3. Section 4 presents and discusses the results. Finally, Section 5 presents the conclusions of the study.

2 OBSERVATIONAL DATA AND THEIR IMPLICATIONS FOR STELLAR STRUCTURE AND EVOLUTION

2.1 Basic properties of the component stars from binary dynamics

In EB light curves, the depths of the eclipses mainly provide information about the $T_{\rm eff}$ of the components, while the widths during the eclipse period and the shape of these widths provide information about the R of the components. The radial velocity curves obtained from the spectroscopic observations also contain information on the masses of the components. These parameters are compiled from the literature and listed in Table 1. References are cited in the last column of the table. We found the results of 15 analyses for the 11 binaries. The components of these binaries are plotted in the Hertzsprung−Russell diagram (HRD, Fig. 1). Although most of the secondary (non-oscillating) components are located around the MS phase, the oscillating RG components have luminosity (L) values around $\log(L/L_\odot) = 1.5 - 2.0$ and $R = 7.65 - 14.0\ R_\odot$.

2.2 Asteroseismic properties of the SLO components

The oscillation frequencies of the SLO components are derived from *Kepler* photometric data (Brown et al. 2011). The frequency at the maximum amplitude of the oscillations ($\nu_{\rm max}$) and the large frequency separation ($\Delta\nu$) are derived from the observations. Note that $\nu_{\rm max}$ is proportional to $g/\sqrt{T_{\rm eff}}$, where g represents gravity (Brown et al. 1991; Kjeldsen & Bedding 1995). Further, $\Delta\nu$ is the average frequency separation between the oscillation modes with the same spherical degree ℓ, but consecutive radial orders n. It is proportional to the square root of the mean density ($\langle\rho\rangle$) of the star (Tassoul 1980; Christensen-Dalsgaard 1993). These parameters of the SLO components are listed in Table 2. For KIC 8410637 (Tek Ayak[1]) and KIC 9540226, the individual frequencies of the oscillation modes with $l = 0$, 1 and 2 are obtained by Themeßl et al. (2018).

The mean of $\Delta\nu$ ($\langle\Delta\nu\rangle$) and $\nu_{\rm max}$ are effective tools for computing the

[1] It is the name of the crow in the Ege University campus that has the ability to live despite having only one leg.

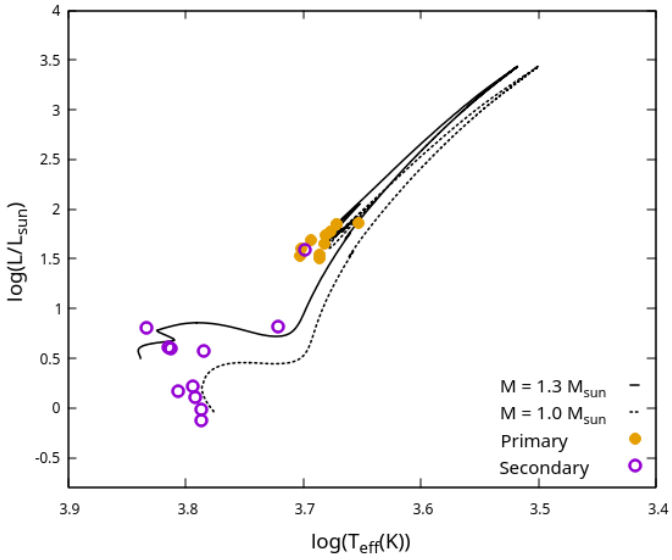

Figure 1. Hertzsprung−Russell diagram (HRD) for the components of the SLO EBs. Filled circles indicate the SLO primaries, while circles indicate the secondary components. The solid and dashed lines show the evolution path from the MS to the RG for the 1.3 and 1.0 $M_\odot$ models, respectively. For these models, the values $Y = 0.2671$, $Z = 0.01$ and $\alpha = 1.8311$ are assumed. Most of the secondary components are in the MS region, while one is in the RG region, and the another is very close to this region. The primary components are concentrated around the RG.

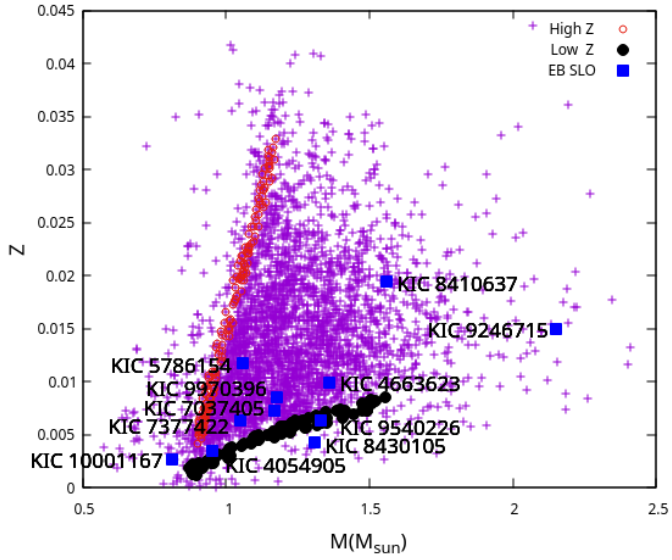

Figure 2. MZ diagram for 11 SLO stars in EBs. The crosses show the masses calculated by Yıldız (2023) from the corrected asteroseismic scaling relation for the Kepler target stars (APKASC-2, Pinsonneault et al. 2018). The effective temperatures and metallicities of these stars are from the APOKASC-2 catalogue, and the corrected distances are from GAIA DR3 (Gaia Collaboration et al. 2021). Squares indicate the oscillating components of the EBs, while circles and filled circles mark the sides of the triangle in the MZ diagram. Most of these stars are located inside the triangle.

Table 1. Observational physical properties of the eclipsing binaries (EBs) with solar-like oscillating (SLO) components. The dynamical values of KIC 4663623, KIC 5786154, KIC 7037405, KIC 7377422, KIC 8430105, KIC 9540226 and KIC 100001167 are taken from Gaulme et al. (2016). Ref. No.: 1 - Brogaard et al. (2022), 2- Gaulme et al. (2016), 3- Brogaard et al. (2018), 4- Frandsen et al. (2013), 5- Themeßl et al. (2018) and 6- Rawls et al. (2016). For three EBs, more than one measurement is available in the literature. The reference numbers in bold indicate the studies from which parameters are taken for modeling the component stars.

KIC	M_A ($M_\odot$)	R_A ($R_\odot$)	M_B ($M_\odot$)	R_B ($R_\odot$)	T_{effA} (K)	T_{effB} (K)	e	P (d)	[Fe/H]	Z_s	Ref
4054905	0.9544 ± 0.0094	8.364 ± 0.027	0.9566 ± 0.0059	3.0911 ± 0.0094	4850 ± 70	5260 ± 240	0.37201	274.7288	-0.60 ± 0.02	0.0034 ± 0.0002	1
4663623	1.36 ± 0.09	9.7 ± 0.2	1.34 ± 0.07	1.82 ± 0.06	4812 ± 92	6808 ± 140	0.43	358.0900	-0.13 ± 0.06	0.0099 ± 0.0013	2
5786154	1.06 ± 0.06	11.4 ± 0.2	1.02 ± 0.04	1.59 ± 0.03	4747 ± 100	6527 ± 138	0.3764	197.9180	-0.06 ± 0.06	0.0117 ± 0.0015	2
7037405	1.25 ± 0.04	14.1 ± 0.2	1.14 ± 0.02	1.80 ± 0.02	4516 ± 36	6303 ± 53	0.238	207.1083	-0.34 ± 0.01	0.0061 ± 0.0001	2
"	1.17 ± 0.02	14.000 ± 0.093	1.110 ± 0.011	1.746 ± 0.014	4500 ± 80	6094 ± 138	0.2364	207.1085	-0.27 ± 0.10	0.0072 ± 0.0015	**3**
7377422	1.05 ± 0.08	9.5 ± 0.2	0.85 ± 0.03	0.87 ± 0.02	4938 ± 110	6120 ± 143	0.4377	107.6213	-0.33 ± 0.06	0.0063 ± 0.0008	2
8410637	1.56 ± 0.03	10.7 ± 0.1	1.32 ± 0.02	1.57 ± 0.03	4800 ± 100	6490 ± 160	0.6864	408.3241	0.16 ± 0.03	0.0194 ± 0.0013	**4**
"	1.472 ± 0.017	10.596 ± 0.049	1.309 ± 0.014	1.556 ± 0.01	4605 ± 80	6066 ± 200	0.686	408.3248	0.02 ± 0.08	0.0140 ± 0.0028	5
8430105	1.31 ± 0.02	7.65 ± 0.05	0.83 ± 0.01	0.770 ± 0.005	5042 ± 68	5771 ± 78	0.2564	63.32713	-0.49 ± 0.04	0.0043 ± 0.0004	2
9246715	2.149 ± 0.007	8.30 ± 0.04	2.171 ± 0.007	8.37 ± 0.05	5030 ± 45	4990 ± 90	0.3559	171.2769	0.05 ± 0.02	0.0150 ± 0.0007	6
9540226	1.33 ± 0.05	12.8 ± 0.1	0.98 ± 0.03	0.99 ± 0.01	4692 ± 65	6399 ± 90	0.3880	175.4439	-0.33 ± 0.04	0.0063 ± 0.0006	**2**
"	1.390 ± 0.031	13.43 ± 0.17	1.015 ± 0.016	1.034 ± 0.014	4585 ± 75	5822 ± 200	0.3877	175.4438	-0.31 ± 0.09	0.0066 ± 0.0012	5
"	1.378 ± 0.038	13.06 ± 0.16	1.002 ± 0.015	1.014 ± 0.014	4680 ± 80	6157 ± 131	0.38782	175.443	-0.23 ± 0.10	0.0079 ± 0.0016	3
9970396	1.178 ± 0.015	8.035 ± 0.074	1.0030 ± 0.0085	1.1089 ± 0.0052	4860 ± 80	6221 ± 125	0.1942	235.2986	-0.20 ± 0.02	0.0085 ± 0.0004	3
10001167	0.81 ± 0.05	12.7 ± 0.3	0.79 ± 0.03	0.98 ± 0.02	4700 ± 66	6191 ± 91	0.159	120.3903	-0.69 ± 0.04	0.0027 ± 0.0002	2

Table 2. Observational asteroseismic properties of the SLO RGs in the EBs. Ref. No.: 1 - Brogaard et al. (2022), 2- Gaulme et al. (2016), 5- Themeßl et al. (2018) and 7- Hekker et al. (2010)

KIC	$\Delta\nu$ μHz	ν_{max} μHz	Ref
4054905	5.404±0.150	48.44±0.55	1
4663623	5.212±0.019	54.09±0.24	2
5786154	3.523±0.014	29.75±0.16	2
7037405	2.792±0.012	21.75±0.14	2
7377422	4.643±0.052	40.10±2.10	2
8410637	4.641±0.017	46.00±0.19	2
"	4.564±0.004	46.4 ±0.3	5
"	4.5±0.1	45.2 ±1.3	7
8430105	7.138±0.031	76.70±0.57	2
9246715	8.310±0.020	106.40±0.80	2
9540226	3.216±0.013	27.07±0.15	2
"	3.192±0.010	26.7 ±0.2	5
9970396	6.320±0.010	63.70±0.16	2
10001167	2.762±0.012	19.90±0.09	2

mass and radius of the oscillating stars. The standard scaling relations for the radius (R_{sca}) and mass (M_{sca}) of an oscillating star are given as

$$\frac{R_{sca}}{R_\odot} = \frac{\nu_{max}/\nu_{max\odot}}{(\langle\Delta\nu\rangle/\langle\Delta\nu_\odot\rangle)^2}\left(\frac{T_{eff}}{T_{eff\odot}},\right)^{1/2}, \quad (1)$$

$$\frac{M_{sca}}{M_\odot} = \frac{(\nu_{max}/\nu_{max\odot})^3}{(\langle\Delta\nu\rangle/\langle\Delta\nu_\odot\rangle)^4}\left(\frac{T_{eff}}{T_{eff\odot}}\right)^{3/2},$$

respectively. Here, $\langle\Delta\nu_\odot\rangle$ and $\nu_{max\odot}$ are the mean values of the solar $\Delta\nu$ and ν_{max}, respectively. $\langle\Delta\nu_\odot\rangle$ = 135.1 and $\nu_{max\odot}$ = 3090 μHz (Sharma et al. 2016).

The non-standard scaling relations (Huber et al. 2017; Li et al. 2022; Yıldız 2023) predict M and R of the SLO components more realistically than the above-mentioned standard relations. In these relations, the correction parameters $f_{\nu_{max}}$ and $f_{\Delta\nu}$ are used to correct the scaling relations ν_{max} and $\Delta\nu$, respectively. To derive the non-standard scaling relations for radius (R'_{sca}), R_{sca} must be multiplied by $f^2_{\Delta\nu}/f_{\nu_{max}}$ as shown below:

$$\frac{R'_{sca}}{R_\odot} = \frac{(\nu_{max}/\nu_{max\odot})}{(\langle\Delta\nu\rangle/\langle\Delta\nu_\odot\rangle)^2}\left(\frac{T_{eff}}{T_{eff\odot}}\right)^{1/2}\frac{f^2_{\Delta\nu}}{f_{\nu_{max}}}. \quad (2)$$

For the non-standard scaling relation for mass (M'_{sca}), M_{sca} should be multiplied by $f^4_{\Delta\nu}/f^3_{\nu_{max}}$:

$$\frac{M'_{sca}}{M_\odot} = \frac{(\nu_{max}/\nu_{max\odot})^3}{(\langle\Delta\nu\rangle/\langle\Delta\nu_\odot\rangle)^4}\left(\frac{T_{eff}}{T_{eff\odot}}\right)^{3/2}\frac{f^4_{\Delta\nu}}{f^3_{\nu_{max}}}. \quad (3)$$

The conventional scaling relations assume that the values of $f_{\nu_{max}}$ and $f_{\Delta\nu}$ are unity. Here, $f_{\Delta\nu}$ can be obtained from the interior models (Sharma et al. 2016), while $f_{\nu_{max}}$ can be determined by comparing R_{sca} and the radius (R_π) computed from the parallaxes. Using data from the APOKASC-2 catalogue and GAIA DR2 data (Gaia Collaboration et al. 2018), Yıldız & Örtel (2021) found that the mean value of $f_{\nu_{max}}$ was 1.003 for the K-mag data of 2MASS (Skrutskie et al. 2006). However, Yıldız (2023) proposed a new parametrisation of $f_{\nu_{max}}$ for RGs and found that $f_{\nu_{max}}$ depends on metallicity, $\Delta\nu$ and effective temperature. This approach is more successful than the method used by Yıldız & Örtel (2021) to predict the M and R of the RGs.

2.3 Mass transfer and the MZ diagram

The MZ diagram plays a crucial role in determining the structural and evolutionary status of RG stars. The MZ diagram constructed by Yıldız (2023) with the mass calculated from the corrected asteroseismic scaling relations for RGs is shown in Fig. 2. Three of the 11 SLO EBs are located outside the triangle in the diagram. The least massive component (KIC 10001167) lost mass (ML side), while the pulsating component of KIC 8430105 gained mass (MG side). Hence, these components are now outside the triangle. In the MZ diagram, the oscillating component of KIC 9246715 is located in the region containing few stars with large masses. The pulsating component of KIC 9540226 is on the baseline of the triangle. Given the uncertainty in the metallicity ([Fe/H]), this star may also be located outside the triangle (see Figs. 7–8).

3 MODEL DESCRIPTIONS AND MODELLING OF THE EB COMPONENTS

It is widely accepted that the component stars of a binary have the same age and chemical composition. The age of the modelled systems depends on the method of computing the chemical composition of the component stars. We constructed interior models for the primary and secondary components using two methods. There are significant differences between the ages of the two components in many cases when an arbitrary chemical composition (for example, solar composition) is involved. The dependence of this difference on the chemical composition is useful for finding a solution for a binary system.

In Method I, we use Z_0 calculated from the observed metallicity of the binaries. The Z_0 values are listed in Table 1. Y_0 can be computed by calibrating the luminosity of component stars of the same age. Subsequently, we determine α_A and α_B by radii calibration. This method is based on the use of observed Z_0. However, there are inconsistencies in the metallicity of some of these binaries as derived from their spectra.

In Method II, we determine the age of the binaries by changing Z by defining a relation between Y_0 and Z_0. We assumed that the chemical enrichment on the galactic disk proceeded as $\Delta Y = 2\Delta Z$, where ΔY and ΔZ are the increases in Y and Z, respectively. Using this method, we determine Z_0 and Y_0 together from the simultaneous luminosity calibration of the components.

MESA code version r23.05.1 (Paxton et al. 2011, 2013, 2015, 2018, 2019; Jermyn et al. 2023) is used to construct nonrotating interior models for the primary and secondary components by two methods. For convection, the standard mixing length theory proposed by Böhm-Vitense et al. (1958) is used. The opacity for the high temperature is computed using OPAL tables (Iglesias & Rogers 1993, 1996), while that for low temperature are taken from Ferguson et al. (2005). Element diffusion is applied using the method proposed by (Paquette et al. 1986). Atmospheric conditions for Methods I and II are computed using the option `table` in the MESA code. The pre-MS phase is included in the construction of the stellar interior models.

In the HRD, the RC region is narrow and perhaps the most degenerate region. Since the stars are not located in a sequence in this region, unlike the MS, many model options exist for a given mass and chemical composition. Therefore, instead of performing precise calibrations in the first stage for RC candidates, we can consider the system age as the age of the primary component in the RG branch. After this point, the transition to an RC occurs rapidly. We then fit the secondary component model to the observational point of the star in the HRD and determine its age (See Fig. 5). There are two important obstacles to determining the age of a binary with an RC component: (a) the unknown amount of mass lost by the star before it reaches the RC region and (b) how much of this lost mass is accreted by the secondary component. Without knowing these unknowns, the age of such binaries cannot be found.

4 RESULTS AND DISCUSSIONS

We calibrate the models for the components of the double-lined binary stars of the 11 EBs. For some of the binaries, more than one result is obtained from the dynamical analysis of the binaries. All the compiled values are listed in Table 1. The values used for modeling are indicated reference numbers in bold in the last column.

Most of the SLO stars in the EBs in the MZ diagram occur around the base of the triangle. Two of them (KIC 5786154 and KIC 8410637) occur significantly above the baseline. Four of them (KIC 4054905, KIC 8430105, KIC 9540226 and KIC 10001167) lie outside or on the border of the triangle. These are candidate stars for mass transfer. The remaining 7 stars can be considered to have possibly evolved with constant mass.

For all binaries, we plotted the HRD with the evolutionary tracks obtained from the grids for certain Z values and the solar value for α. For this grid, Y is computed using the chemical enrichment law with $c = 2$: $Y = Y_p + 2Z$. The HRDs of six binaries are shown in Fig. 3. For four binaries (KIC 4663623, KIC 8410637, KIC 8430105 and KIC 10001167), the evolutionary tracks of the components pass either through or very close to their observed positions in the HRD. However, this does not imply the existence of a simultaneous solution for these systems. Importantly, the evolutionary tracks of the components pass near the observed position at similar times. For two systems, KIC 5786154 and KIC 73777422, the tracks and the observed positions are slightly further apart. For the second component of KIC 5786154, the model luminosity is slightly higher than the observed value. These discrepancies can be resolved by increasing the modelled Y for a given Z or decreasing the modelled Z for a given $Y - Z$ relationship. The value of α of the secondary component is as important as Y and Z to ensure agreement between the observed position and the evolutionary track of KIC 73777422 B.

The primary and secondary components of three of the 11 binaries, namely, KIC 4054905, KIC 4663623 and KIC 9246715, have masses so similar that Methods I and II are not applicable. The primary component of KIC 4054905 has less mass and a larger radius than the secondary component. This is a strong indication of mass transfer between the components or mass loss of the primary component. For these systems, the solution is found only from the interior models of the primary components. The ages of KIC 4054905, KIC 4663623 (see also Section 4.3.7) and KIC 9246715 are found to be 9.328, 3.28 and 0.782 Gyr, respectively.

Four of the six SLO stars shown in Fig. 3 are inside the triangular region in the MZ diagram (Fig. 2), while the remaining two, KIC 8430105 and KIC 10001167, are outside the triangle. KIC 8430105 is on the MG side, while KIC 10001167 is on the ML side of the triangle. For such systems, the solutions obtained by Methods I and II are approximate. The results for the systems with the primary component within the MZ triangle are much more accurate than those for the systems outside the triangle.

4.1 Results obtained by Method I: Finding age by changing Y_0

For the application of Method I, we initially take α_A=α_B=$\alpha_\odot$ because α has very little affect on the luminosity of a model at any given time. Z is calculated from the spectroscopically determined [Fe/H]. Note that it is necessary but not sufficient to fit the component stars of a binary in the HRD alone. For the components to be synchronous, t_{9A} must be equal to t_{9B}. Both ages are functions of Y_0. However, the age of the secondary components is a more sensitive function of Y_0 than that of the primary star. In Fig. 4a, the difference between t_{9A} and t_{9B} is plotted against Y_0 for the KIC 7377422 system. A linear relationship exists between $t_{9A} - t_{9B}$ and Y_0. Note that $t_{9A} - t_{9B}$ equals zero at Y_0=0.2868. The corresponding age for this Y_0 is 5.79 Gyr (Fig. 4b and Table 3). From the calibration of the radii of the components, we find that α_A = 2.1731 and α_B = 2.1401.

Method I is also applied to the other EBs. The results are summarised in Table 3. For three EBs (KIC 4054905, KIC 4663623, and KIC 9246715), no solution is obtained. In addition to these binaries, the solution of KIC 10001167 had a very small Y_0. The second solution with Z_0=0.0057 for KIC 5786154 seems more reasonable than the first solution (see also solution with Method II).

From the coevality constraint, Method I yielded Y_0 values of 0.2381−0.3039. Of these systems, only the Y_0 of KIC 7037405 is less than the primordial Y_p value. While the age of the youngest system (Tek Ayak) is 2.17 Gyr, the oldest system is KIC 7377422, with an age of 5.79 Gyr. The ranges of α_A and α_B are 1.7811−2.2358 and 1.4311−2.5666, respectively.

4.2 Results obtained by Method II: Finding age by changing Z_0

Using Method II, we calibrated the models for the components of eight double-line spectroscopic binary (SB2) stars for which sufficiently precise observational data are available. We calculated the parameters of each system by applying the above-described method. The collective results are summarised in Table 3.

To explain the basics of the method, we again consider the model calibration of the component stars of KIC 7377422. For the component models in the HRD for this binary, Z = 0.0075 is assumed in Fig. 3. There is a significant difference between t_{9A} and t_{9B} for this Z value: t_{9A}-t_{9B} =−2.475 Gyr if we assume the primary component as an RG star and −2.407 Gyr if we assume an RC star. For a given Y-Z relationship, the only way to fix the age difference is to drop Z (Z < 0.0075). The agreement should be at the same age. The t_{9A}-t_{9B} differences for other Z_0 values are plotted in Fig. 5. As Z decreases, the difference increases. When Z_0=0.00382 for RG, t_{9A} becomes equal to t_{9B}. For the two ages of the RC model to be equal, we need Z_0 = 0.00402.

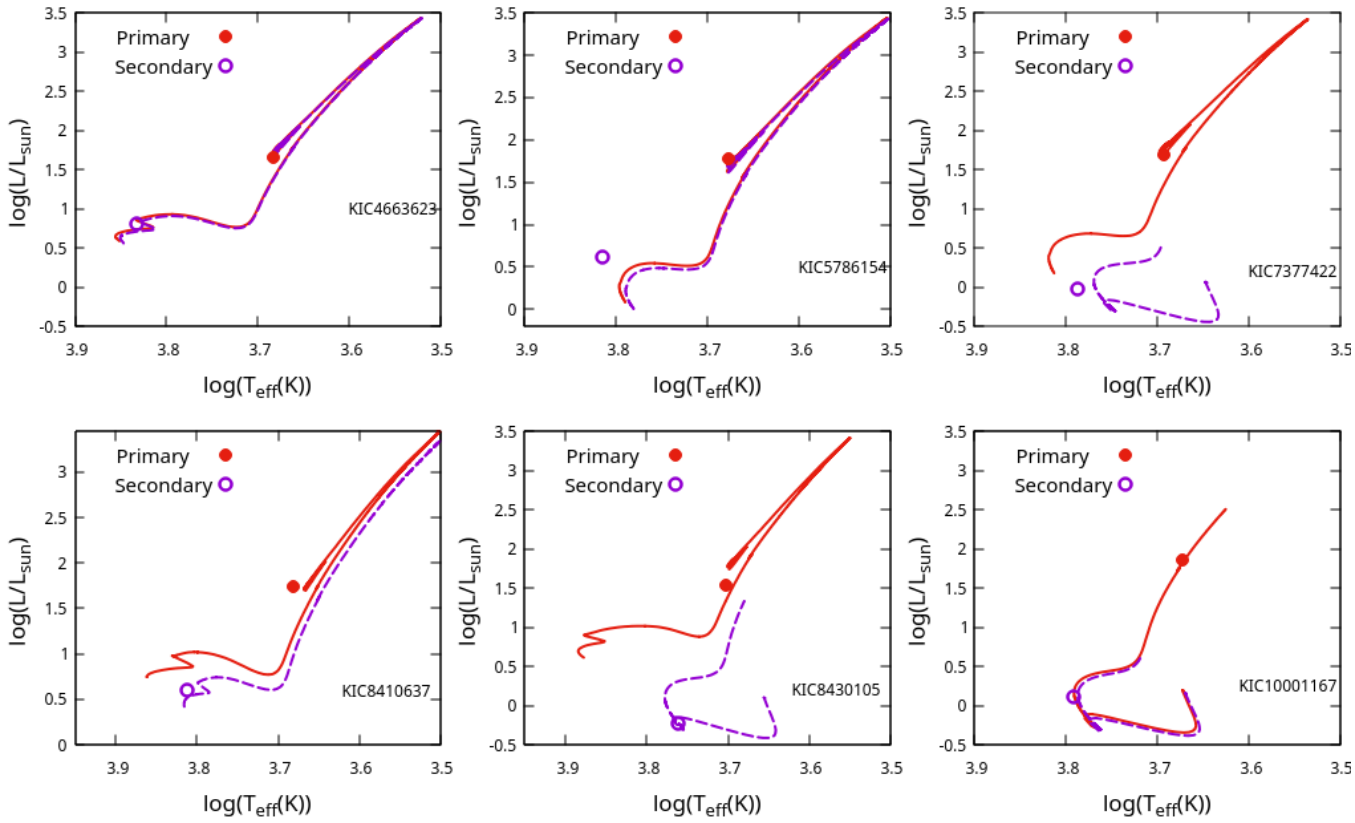

Figure 3. HRD of the components of the SLO EBs. The filled circle represents the primary, and the circles represent the secondary components. The evolutionary tracks are obtained from the grids nearest to the observed values of masses (M_A and M_B) and metallicity (Z). The filled circles represent two different sets of observations. Since the value of the Sun is used as the mixing length parameter in these evolution grids, there may be temperature differences between the evolutionary traces and the observational points. In terms of luminosity, while the secondary component of five of these 6 stars is around MS, one of them (KIC 5786154) has a higher luminosity than MS the Z of this system must be lower than the observed value.

The two Z_0 values obtained for the RG and RC cases are very close because the transition from RG to RC occurs rapidly. In Fig. 5b, the age of component A is plotted according to Z_0 values. According to Z_0 values, we find that the age of the system is 6.145 Gyr for RG case and 6.290 Gyr for the RC case.

After these solutions are obtained for luminosity, we also matched the $T_{\rm eff}$ values by changing the α parameter. There is a slight difference in the age difference because of changes in α. In this case, we also recalculated Z. Our final results obtained with iterations are provided in the lower part of Table 3. The final parameters of the KIC 7377422 system are $Z_0 = 0.00368$, $t_9 = 6.13$ Gyr, $\alpha_A = 2.0129$ and $\alpha_B = 1.9412$.

Method II yields $Y_0 = 0.2545-0.2797$, which is much narrower than the Y_0 range obtained by Method I. The Y_0 of all the systems exceeds the primordial Y_p value. While the age of the youngest system (Tek Ayak again) is 2.30 Gyr, the oldest system is KIC 7377422, with an age of 6.13 Gyr.

The main source of uncertainty for RC models is the unknown amount of mass lost. We can simplify the situation and obtain interior models with a constant mass. For a more realistic RC model, another important factor is the amount of mass the second component gains.These discussions can be the subject of another study (Örtel & Yıldız 2025, in preparation).

The model asteroseismic properties of the primary components of the 7 EBs are compared with the observational values in Fig. 6. The upper panel shows $\Delta\nu$ and the lower one shows $\nu_{\rm max}$. Both Methods I and II yield very similar results. The $\Delta\nu$ of the models are in good agreement with the observed $\Delta\nu$. Furthermore, the $\nu_{\rm max}$ values also agree, but a slight scattering is observed.

The uncertainties in the model results Table 3 are computed by different methods. The uncertainty in Z_0 in Methods I and II is computed from the observational [Fe/H] value using the equation $Z = 10^{[Fe/H]}0.0134$. To compute the uncertainty in Y_0, the average of the c_{YZ} coefficient in Methods I and II is taken and multiplied by the uncertainty in Z_0. The average c_{YZ} values for Methods I and II are 2.7 and 2, respectively. Typical uncertainties in age are computed from the age−mass relation ($t_9 \propto M^{-2.5}$).

The uncertainty in $\Delta\nu$ and $\nu_{\rm max}$ is estimated by Monte-Carlo simulation using the observational values of M, R and $T_{\rm eff}$ given in Table 1. In the Monte-Carlo simulation, 1000 synthetic data are generated for each parameter within the uncertainty limits. The $\Delta\nu$ and $\nu_{\rm max}$ values are computed from the synthetic data generated. The standard deviation computed from the 1000 synthetic data is taken as the uncertainty.

4.3 Notes on the individual SLO binaries

4.3.1 KIC 5786154

Using the Z value of KIC 5786154 given in Table 1, we constructed the interior models for the component stars with different Y_0 by applying Method I. We found that $t_{9A} = t_{9B} = 4.83$ for $Y_0 = 0.3484$. From radii calibration, $\alpha_A = 2.1451$ and $\alpha_B = 2.9911$. The values for Y_0 and $\alpha_B = 2.9911$ are very high.

The highest difference between the Z obtained from Method II models (0.0117) and the observational Z (0.00392) occurs for this star. Table 4 lists the spectral data of this star obtained from the Simbad database (Wenger et al. 2000). The data given by Gaulme et al. (2016) are provided in the last row of the list the highest temperature was obtained in this study. In general, the spectral data of a star show an interesting feature: the $T_{\rm eff}$, $\log g$ and

Table 3. Solutions obtained with Methods I and II for the eight EBs from the interior models of the component stars. The model luminosities are only equal to the observational ones for a single Y_0 (Method I) or Z_0 (Method II) value. The second and third columns list Z_0 and Y_0, respectively. The primary components are assumed to be RG. The corresponding age (t_9) is listed in the fourth column. The α_A and α_B values obtained from the fit of the model $T_{\rm eff}$ with the observational $T_{\rm eff}$s are given in the fifth and sixth columns. The factor for the chemical enrichment law between Z and Y, c_{YZ} is given in the seventh column: $Y_0 = Y_p + c_{YZ}Z_0$. Columns 8−11 list modelled and observed values of $\nu_{\rm max}$ and $\Delta\nu$.

KIC ID	Z_0	Y_0	t_9	α_A	α_B	c_{YZ}	$\nu_{\rm max}$(model) μHz	$\Delta\nu$(model) μHz	$\nu_{\rm max}$ μHz	$\Delta\nu$ μHz
Method I										
5786154	0.0117 ± 0.0015	0.3484 ± 0.0041	4.83 ± 0.68	2.1451	2.9911	8.66	29.46±1.97	3.549±0.136	29.75±0.16	3.523±0.014
"	0.0057 ± 0.0015	0.2803 ± 0.0041	5.67 ± 0.80	1.9544	2.5666	5.83	28.41±1.92	3.516±0.133	29.75±0.16	3.523±0.014
7037405	0.0072 ± 0.0015	0.2381 ± 0.0041	5.75 ± 0.25	1.7811	1.4311	-1.30	20.74±0.47	2.692±0.035	21.75±0.14	2.792±0.012
7377422	0.0063 ± 0.0008	0.2868 ± 0.0022	5.79 ± 1.10	2.1731	2.1401	6.30	39.74±3.44	4.604±0.199	40.10±2.10	4.643±0.052
8410637	0.0194 ± 0.0013	0.3039 ± 0.0035	2.17 ± 0.10	2.2358	2.0696	2.93	48.00±1.39	4.673±0.079	46.00±0.19	4.641±0.017
8430105	0.0043 ± 0.0004	0.2482 ± 0.0011	3.08 ± 0.12	1.9311	1.8123	0.25	74.12±1.53	7.103±0.088	76.70±0.57	7.138±0.031
9540226	0.0063 ± 0.0006	0.2740 ± 0.0016	2.81 ± 0.26	1.8311	2.0102	4.28	28.26±1.18	3.353±0.075	27.07±0.15	3.216±0.013
9970396	0.0085 ± 0.0004	0.2633 ± 0.0011	5.04 ± 0.16	2.0218	1.8935	1.91	62.12±1.44	6.236±0.093	63.70±0.16	6.320±0.010
10001167	0.0027 ± 0.0002	0.1518 ± 0.0005	—	—	—	-35.3	—	—	19.90± 0.09	2.762± 0.012
Method II										
5786154	0.0039 ± 0.0015	0.2549 ± 0.0030	6.04 ± 0.85	1.8311	2.2940	2.00	28.01±1.89	3.511±0.136	29.75±0.16	3.523±0.014
7037405	0.0093 ± 0.0015	0.2657 ± 0.0030	5.42 ± 0.23	1.8619	1.5848	2.00	21.22±0.48	2.703±0.035	21.75±0.14	2.792±0.012
7377422	0.0037 ± 0.0008	0.2545 ± 0.0016	6.13 ± 1.17	2.0129	1.9412	2.00	39.14±3.44	4.629±0.229	40.10±2.10	4.643±0.052
8410637	0.0163 ± 0.0013	0.2797 ± 0.0026	2.30 ± 0.11	2.1884	1.9175	2.00	47.47±1.39	4.695±0.081	46.00±0.19	4.641±0.017
8430105	0.0051 ± 0.0004	0.2572 ± 0.0008	3.03 ± 0.12	1.9908	1.8599	2.00	74.70±1.52	7.110±0.083	76.70±0.57	7.138±0.031
9540226	0.0048 ± 0.0006	0.2566 ± 0.0012	2.88 ± 0.27	1.9073	1.7540	2.00	28.08±1.11	3.366±0.071	27.07±0.15	3.216±0.013
9970396	0.0086 ± 0.0004	0.2642 ± 0.0008	5.03 ± 0.16	2.0245	1.8763	2.00	62.49±1.48	6.260±0.095	63.70±0.16	6.320±0.010
10001167	0.0092 ± 0.0002	0.2655 ± 0.0004	19.81 ± 3.06	> 4	2.4384	2.00	—	—	19.90±0.09	2.762±0.012

Table 4. Spectral data for the KIC 5786154 system according to the Simbad database.

$T_{\rm eff}$(K)	log g (cgs)	[Fe/H]	Ref.
4642	2.579	-0.178	Qian et al. (2018)
4620	2.56	-0.160	"
4610	2.59	-0.140	"
4610	2.70	-0.030	"
4606	2.60	-0.148	Zhang et al. (2019)
4514	2.53	-0.13	Frasca et al. (2016)
4747	2.60	-0.06	Gaulme et al. (2016)

[Fe/H] values mostly form a plane in a three-dimensional graph. Without including these data, the coefficients obtained from the data in Table 4 using the relationship [Fe/H]= $f(x, y) = bT_{\rm eff} + c\log(g)$ are as follows:

$$f(x, y) = -(5.65 \pm 0.71) \times 10^{-4} T_{\rm eff} + (0.95 \pm 0.13)\log(g)$$

When the $T_{\rm eff}$ values are around 4610 K, the log g calculated from the orbital analysis is 2.35 (cgs). Using these values, we find the possible value for [Fe/H] (−0.37). For this [Fe/H] value, $Z = 0.0057$. Further, the value obtained by Method II is 0.0039. These two values are very compatible with each other.

4.3.2 KIC 8410637 (Tek Ayak)

While Gaulme et al. (2016) and previous studies suggest that the primary component of this system may be an RC star (Hekker et al. 2010; Gaulme et al. 2016; Brogaard et al. 2016), Themeßl et al. (2018) confirm that it is an RG star.

Data were obtained from two studies on the KIC 8410637 system (Frandsen et al. 2013; Themeßl et al. 2018). We use the data of Frandsen et al. (2013) in modelling the components. The oscillation frequencies are given in Themeßl et al. (2018).

The primary component of KIC 8410637 can be considered a unit star (see Fig. 10) in asteroseismic relations (Eqs. 1−3). Therefore, it is useful to give detailed model features: $Z_0 = 0.01629$, $Y_0 = 0.2797$, $t_9 = 2.30$, $\alpha_A = 2.1884$, $Y_s = 0.29254$, $Z_s = 0.01638$, $X_s = 0.69108$, $T_{\rm eff} = 4800$, $R = 10.69$ R$_\odot$, $\Gamma_{1s} = 1.6523$ and $\mu_s = 1.3163$. The last two parameters introduce the scaling relations over $\nu_{\rm max}$.

We construct an interior model for the primary component using the MESA astero module and obtain the adiabatic oscillation frequencies to compare the observed frequencies. In this module, the near-surface effects on the frequencies are computed using the 'combined' option of Ball & Gizon (2014). The observed and model oscillation frequencies are in excellent agreement.

4.3.3 KIC 9540226 (Ayya)

The parameters of the components of KIC 9540226 are obtained in three studies (Gaulme et al. 2016; Brogaard et al. 2018; Themeßl et al. 2018). In these studies, high-quality light curves and radial velocity measurements of KIC9540226 are analysed. The uncertainties in radii are the smallest in Gaulme et al. (2016). The dynamic mass and radius given by Gaulme et al. (2016) are used in our model computations. In Themeßl et al. (2018), the oscillation frequencies of the primary component are detected and its RG nature is reported. The ages determined by Methods I and II are in very good agreement. In the MZ diagram, the primary component is very close to the triangle base. The Z_0 value obtained by Method II suggested that the star might have gained mass in the past.

4.3.4 KIC 7037405

Z_0 is determined to be 0.0093 by Method II. This value agrees well with the metallicity found from APOGEE DR12 ([Fe/H] = −0.13). The difference between the ages obtained by Methods I and II is approximately 6%. The results obtained by Method II are more reasonable because the Y_0 in Method I is less than Y_p. According to Methods I and II, the age of the system is 5.75 and 5.42 Gyr, respectively. Despite the very different chemical compositions obtained by the two methods ($(Z_0, Y_0) = (0.0072, 0.2381)$ for Method I and

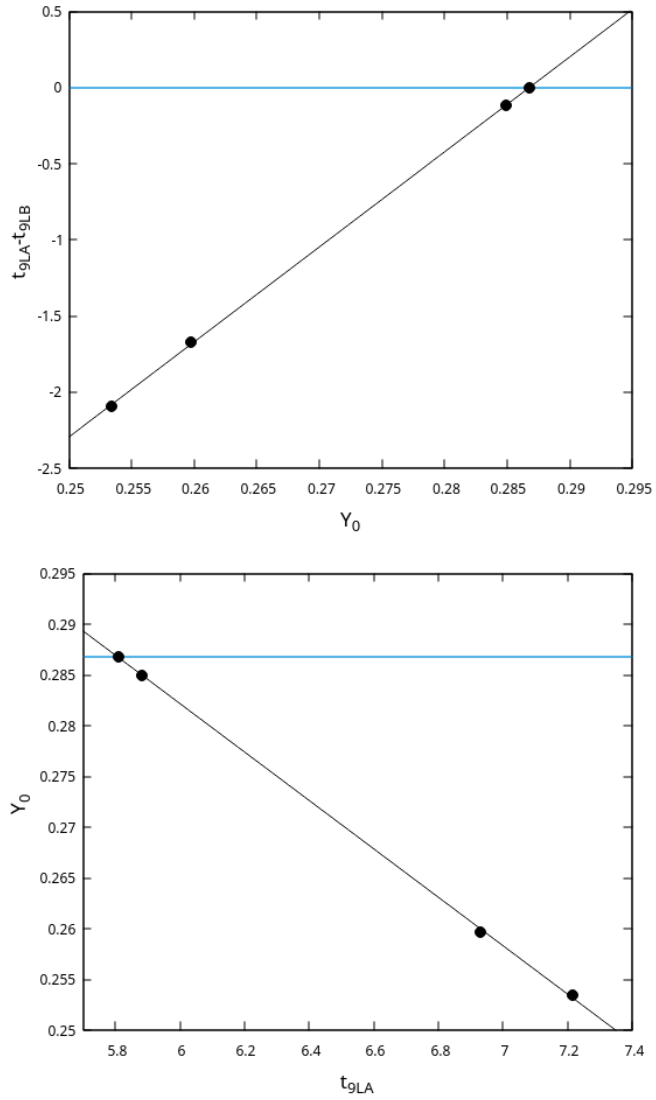

Figure 4. a) Age difference between the components of KIC 7377422 is plotted with respect to Y_0 (Method I). For the coevality of the components, $Y_0 = 0.2868$. b) The corresponding age of the system is found to be 5.79 Gyr.

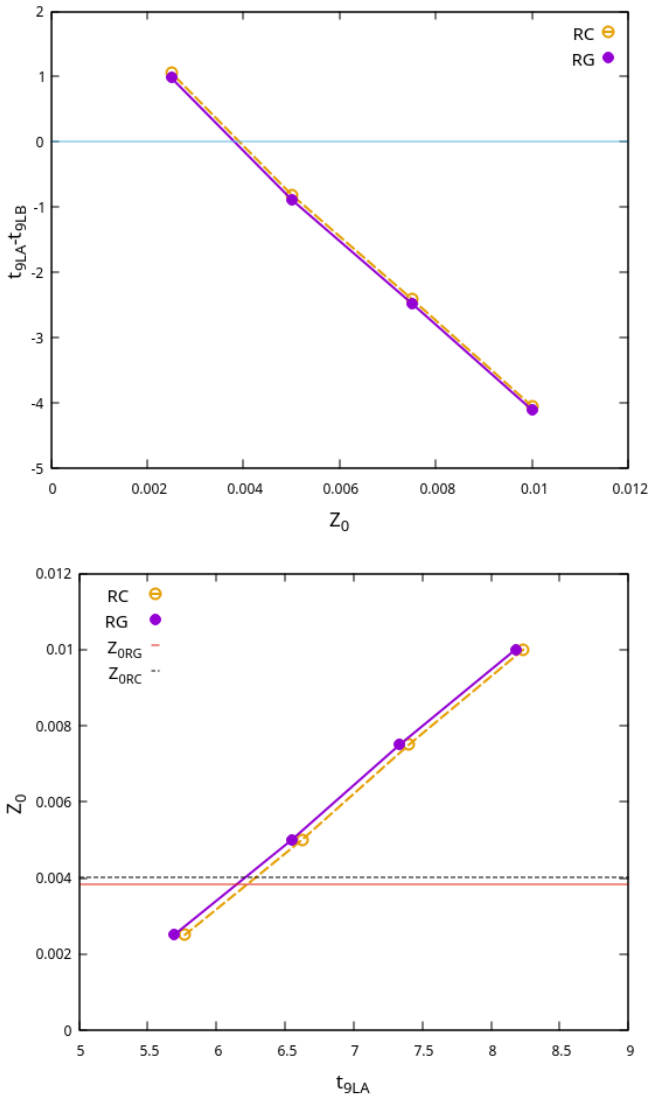

Figure 5. a) Age difference between the components of KIC 7377422 is plotted with respect to Z_0 (Method II). We obtain two solutions based on the evolutionary phases of the primary component. The circles and filled circles represent the RG and RC phases, respectively. For the coevality of the components, $Z_0 = 0.0037$. b) The corresponding age of the system is found to be 6.13 Gyr.

(0.0093, 0.2657) for Method II) it is interesting that the obtained ages are very close.

4.3.5 KIC 9970396

The parameters of the system (Z_0, Y_0, t_9 and αs) obtained by Methods I and II are in perfect agreement. The differences between the values derived by these methods are negligibly small. The value of c_{YZ} obtained by Method I is 1.91, very close to two. The primary component of this system can also be used as a unit star in the scaling relations for RGs (see Fig. 10).

4.3.6 KIC 4054905

Solar-like oscillations are detected in four EB stars by Benbakoura et al. (2021). They stated that the primary component of the KIC 4054905 system is an RC star. No common solution for age and chemical composition is available for this system. Only a rough estimate of the age is obtained using the interior model of the primary component: about 9.3 Gyr.

4.3.7 KIC 4663623

The fundamental properties of the components of KIC4663623 are obtained by Gaulme et al. (2016) and Benbakoura et al. (2021). The mass of both components ($1.41 M_\odot$) is the same as that reported in the data of Benbakoura et al. (2021). We prefer to use the data reported by Gaulme et al. (2016).

The most interesting aspect of this system is that although the masses of the two stars are very close to each other, the primary component seems to have evolved a lot, whereas the secondary component seems to have evolved very little. Therefore, it is not possible to find a common age. If the observational data are reliable, mass transfer must have occurred.

It is possible that the primary star is an RC and has lost a significant amount of mass before reaching this region in the HRD. We can estimate this amount of lost mass. For this purpose, we find the estimated age of the secondary component by modelling. For $Z_0 = 0.01$, $t_{9B} = 2.63$ Gyr. At this age, we can determine at what mass the primary component model satisfies

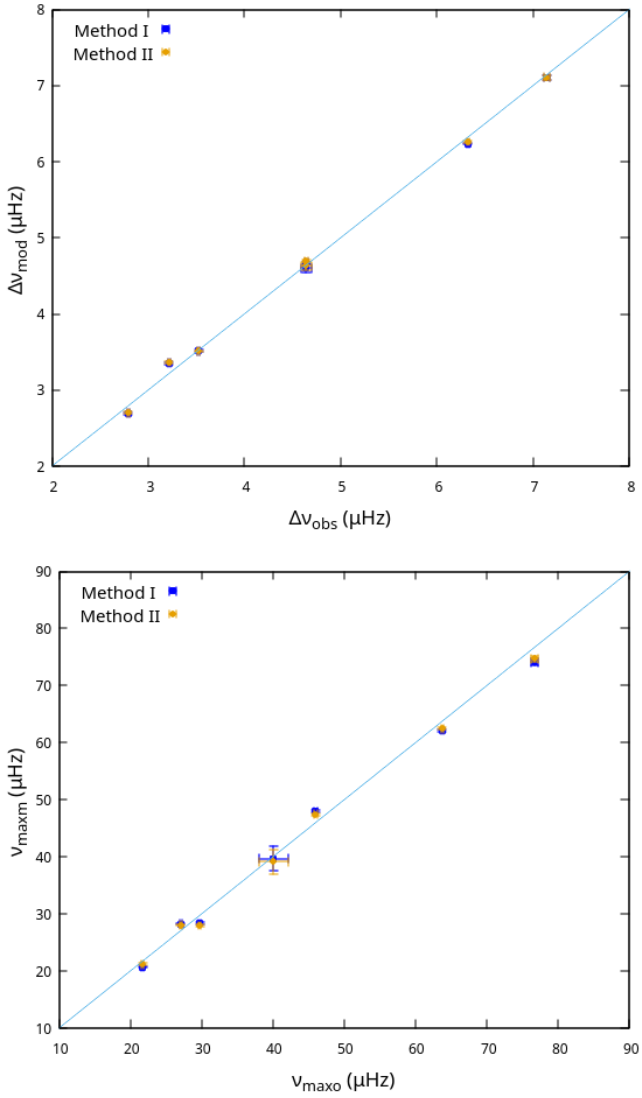

Figure 6. Comparison of the modelled and the observed a) $\Delta\nu$ and b) $\nu_{\rm max}$. The square represents the case for models with Method I and the circle represent the case of the models with Method II.

the condition $L = L_{\rm A}$. This mass turns out to be around 1.45 $M_{\odot}$. In this case, we determined the amount of mass loss: $\Delta M = 1.36 - 1.45 = -0.09$ $M_{\odot}$.

4.3.8 KIC 9246715

Both components in this system are located in the RC region on the HR diagram, and the values of M (2.15) and R (R 8.30) are very close to each other (Gaulme et al. 2016).

The dynamical and asteroseismic parameters of the stars are taken from Gaulme et al. (2016). The period gap ($\Delta\Pi$) and $\Delta\nu$ of the primary component in the KIC 9246715 system were determined to be 150 s and 8.310 μHz, respectively, by Gaulme et al. (2020). According to these values, the primary component is an RC star (Frandsen et al. 2013; Rawls et al. 2016).

Constructing the interior models of the components of such a binary system with an RC component is a difficult task. In this case, there are two important sources of uncertainty: (a) the mass lost by the RC component and (b) the mass gained by the other component from this lost mass. The approximate

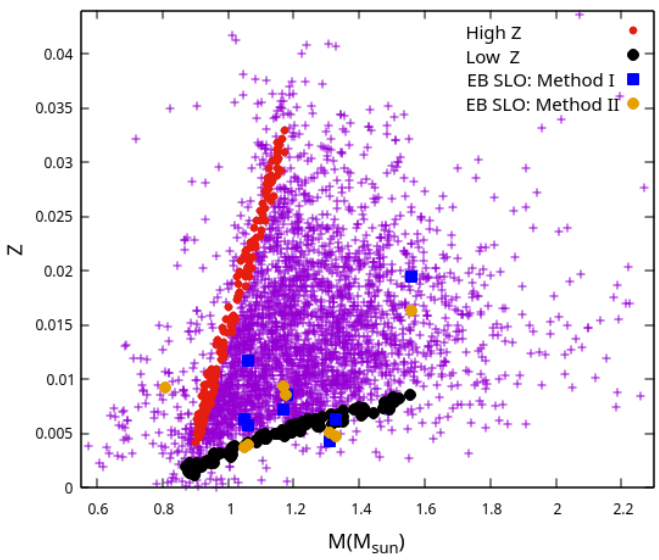

Figure 7. MZ diagram for 8 SLO RGs in EBs. The big filled circles and filled squares indicate the results obtained using Methods I and II, respectively. The oscillating components of the EBs. Most of these stars are located inside the triangle. While KIC 10001167 is on the ML side, KIC 8430105 and KIC 9540226 are on the MG side.

age determined using the interior model of the primary component is about 0.8 Gyr.

4.3.9 KIC 10001167

The dynamical and asteroseismic parameters of the stars are given in Gaulme et al. (2016). The primary component of this star lies on the left side of the triangle on the MZ diagram. In this case, the primary component has definitely lost mass. We first constructed interior models of the components with a constant mass and with $Z = 0.0027$. There is a discrepancy between the model ages of the components. The age of the low-mass star is 12 Gyr, whereas that of the seismic component is 7 Gyr. The large discrepancy is removed when we take a very small value of Y_0 (0.1518 in Method I). The solution obtained by applying Method II has a relatively high Z (0.00921) and indicates very high age (19.81 Gyr). This age is larger than the age of the Milky Way (13.4 Gyr; Gratton et al. 2003). These extreme values of Y_0, Z_0 and age show that in such binaries, experienced mass transfer, modelling with a constant mass is inaccurate.

4.3.10 KIC 7377422

The dynamical and asteroseismic data for the components are taken from Gaulme et al. (2016). We obtained the solutions for the stellar parameters by applying both Methods I and II. The ages determined by Methods I and II are 5.79 and 6.13 Gyr, respectively. The Y_0 (0.2868) obtained by Method I is very high for $Z_0 = 0.0063$, yielding a very high value for c_{YZ} (6.30).

4.3.11 KIC 8430105

This system has the minimum mass ratio among the 11 EBs: $q = M_{\rm B}/M_{\rm A} = 0.634$. The ages found by Methods I and II are very close to each other. However, c_{YZ} (0.25) obtained by Method I is very small for this system.

According to the results of Method II, the three stars of the system are outside the triangle in the MZ diagram. Two of them are very far from the triangle one of these stars, KIC 10001167, appears to have lost a significant mass, while the other, KIC 8430105, appears to have gained mass. The third

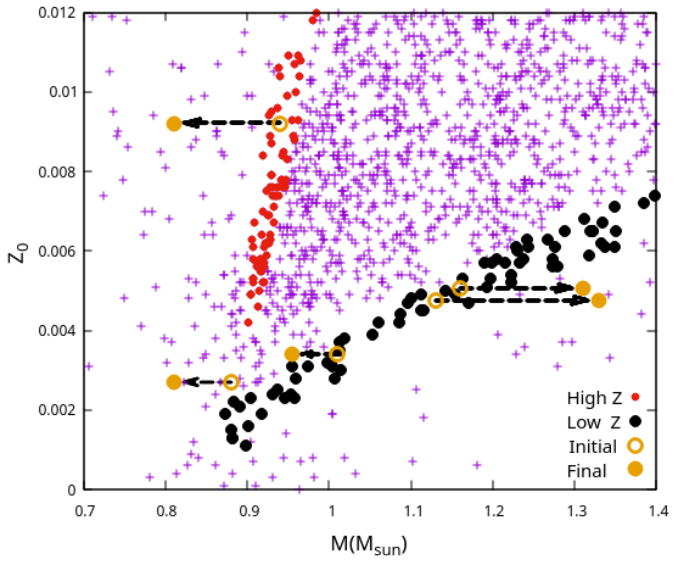

Figure 8. Initial and final positions of the stars gaining and losing mass in the MZ diagram. The big circles and big filled circles represent the initial and final positions of the stars, respectively.

star, KIC 9540226, also appears to have gained mass. Notably, the mass gain of a component in a binary system does not prevent us from determining the chemical composition and age of the system (see Section 4.4).

4.4 Finding stars gaining and losing mass from the analysis based on the MZ diagram

We obtaine very clear findings regarding the mass transfer in four of the SLO stars. In one of these stars, KIC 4054905, the mass of the evolved SLO component is smaller than that of the less-evolved second component. Such a result cannot occur without mass transfer. Since the rate of evolution of two components with the same chemical composition depends very strongly on the mass, the initial mass of component A must be greater than it is now. A typical value for how much mass component A may have lost can be obtained from the MZ diagram.

The MZ diagram shows strong indications of the mass change of the other three stars in the MZ diagram. All three of these stars are located outside the triangle in the diagram. The first component in the KIC 10001167 system is located on the left side of the triangle and has suffered a very serious mass loss, 0.13 $M_\odot$. If it had evolved with its current mass without losing mass, it would have reached its current level of evolution only in about 19 billion years. Since this age is much larger than the age of the galaxy, the initial mass must be greater than the current one.

The primary components of the other two EBs are located below the triangle in the MZ diagram. These stars should have already evolved and left the RG region. These systems were most likely triple system, and the current primary component reached its current mass by partly or entirely swallowing the third component closest to it. In particular, the RG component in KIC 9540226 should have gained a mass of at least 0.2 $M_\odot$. In this case, the initial mass must be around $M_{\rm Ai}$ = 1.13. The other mass-gaining system, KIC 8430105, may have gained a mass of at least 0.15 $M_\odot$. Hence, mass-gaining models should be developed for these systems. In this case, a result may be obtained by an extended iteration process.

The displacements of these systems in the MZ diagram are shown in Fig. 8. Arrows to the left indicate mass loss, and those to the right show mass gain. The mass changes determined from this diagram are listed in Table 5.

Table 5. Estimated mass loss and mass gain in four EBs. These values are obtained from the MZ diagram and can be considered as the minimum values.

KIC	$M_{\rm A}$ ($M_\odot$)	$M_{\rm B}$ ($M_\odot$)	$M_{\rm Ai}$ ($M_\odot$)	$M_{\rm Bi}$ ($M_\odot$)	$M_{\rm A} - M_{\rm Ai}$ ($M_\odot$)	MT
4054905	0.9544	0.9566	1.01	0.938	-0.0556	ML
10001167	0.81	0.79	0.94	0.746	-0.13	ML
8430105	1.31	0.83	1.16	0.83	+0.15	MG
9540226	1.33	0.98	1.13	0.98	+0.20	MG

4.5 Mass accretion by the secondary component from the mass lost by the primary component: KIC 10001167 and KIC 4054905 systems

If the primary component gains mass, we can assume that the mass of the secondary component does not change because the secondary components of KIC 9540226 and KIC 8430105 appear to be normal MS stars. In the case that the primary component loses mass, the masses of the secondary components may not be constant. In KIC 10001167 ($M_{\rm A}$ = 0.81 and $M_{\rm B}$ = 0.79 $M_\odot$), for Z_0=0.00921, $M_{\rm Ai} = M_{\rm A} + 0.13 = 0.94$ $M_\odot$. The greatest obstacle to finding a solution for such systems is that we do not know how much of the mass lost by the primary is transferred to the secondary component. Yıldız & Doğan (2013) examined the W UMa systems and found that $(1 - 0.664) = 0.336$ of the mass lost by the primary is transferred to the secondary component. If the same situation exists in the case of the SLO EBs, then $M_{\rm Bi} = M_{\rm B} - (1 - 0.664)0.13 = 0.79 - 0.044 = 0.746$ $M_\odot$. Because the components of these systems are not as close together as in the W UMa-type binaries, the amount of mass transferred to the secondary component may be less than the values stated above.

Using the metallicity of the system obtained from the [Fe/H] value (Z_0 = 0.0027), we found that $M_{\rm Ai}$ = 0.85 $M_\odot$ for the common age from the mass loss models we developed. For Z_0 = 0.0037, $M_{\rm Ai}$ = 0.84 $M_\odot$. We obtained a solution from the intersection of the line representing the left side of the triangle and the line representing the $M - Z$ relationships for the models Z_0 = 0.0010, $M_{\rm Ai}$ = 0.867 $M_\odot$. For this solution, the age of the system is 10.08 Gyr. This value is acceptable as it does not exceed the age of the galaxy. The solution we obtained by considering the line representing the base of the triangle is Z_0 = 0.0017, $M_{\rm Ai}$ = 0.860 $M_\odot$.

4.6 Chemical evolution

The solutions we obtained from the non-asteroseismic data of the EBs are already listed in Table 3.

In the upper and lower panels of Fig. 9, Y_0 and metallicities ($Z_0 + 0.008$) of the 7 EBs as obtained from Methods I and II are plotted against age on logarithmic scales, respectively. Despite the scattering, there is a clear relationship between Y_0 and age. This relationship is consistent with the initial Y (Y_P) of the galaxy. The galaxy is set to 13.4 Gyr old and Y_P = 0.2471. The initial Z of the galaxy is assumed to be zero. The constant 0.008 is arbitrarily added to the vertical axis to avoid the undefinedness of $\log(Z = 0)$. The four points around $\log(Z + 0.008) = 0.47$ for the mass-gaining EBs. We obtained a clear age-metallicity relationship for the remaining five systems. The circle at the bottom right corner in the lower panel represents the initial $Z = 0$ condition of the galaxy. These relationships show how the chemical enrichment of these EBs depends on time.

4.7 Asteroseismic analysis

We calculate the adiabatic oscillation frequencies of the internal structure models that satisfy the non-asteroseismic observational constraints using the ADIPLS package in MESA. We also calculate $\Delta\nu_{\rm mod}$ from these frequencies. We compute $\nu_{\rm max}$ using the values of Γ_1, μ, g, and $T_{\rm eff}$ of the model and $\Delta\nu_{\rm sca}$ from the mean density. The values show good agreement, in general. We obtaine a similar situation in the $\nu_{\rm maxm} - \nu_{\rm maxo}$ relationship (Fig. 6).

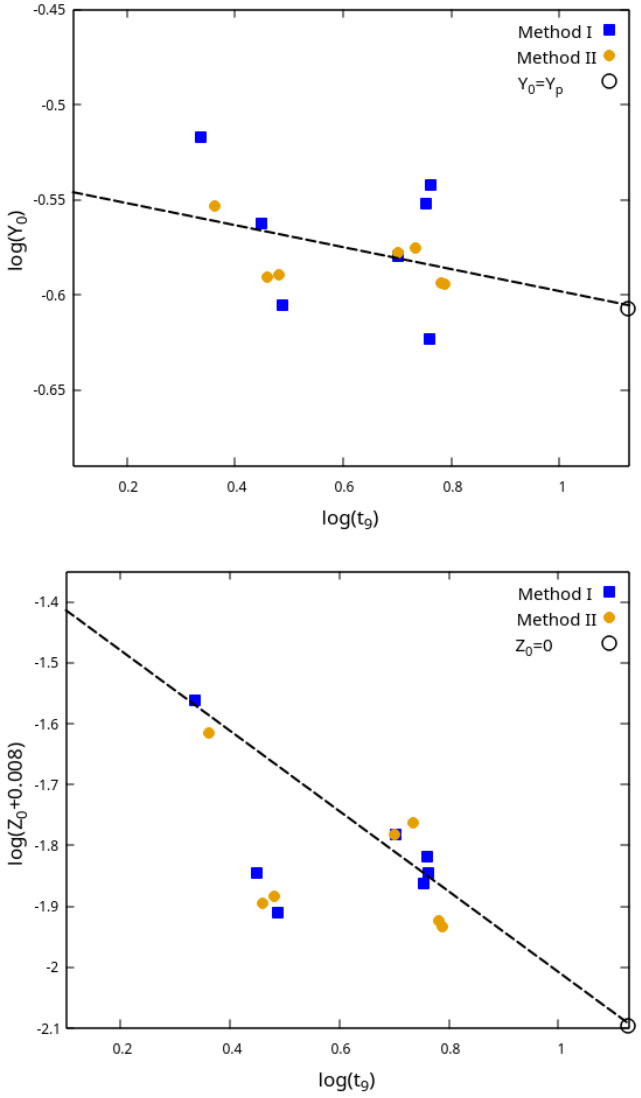

Figure 9. The age−Y and age−metallicity relations. (a) $\log(Y_0)$ of the EBs from Methods I (filled squares) and II (filled circles) are plotted with respect to $\log(t_9)$. The dotted line represents the fitted line. The primordial Y_p value (circle) is in excellent agreement with this fitted function. The minimum value of Y is assumed to be 0.2471 (Planck Collaboration et al. 2020) at $t_9 = 13.4$. (b) $\log(Z_0 + 0.008)$ is plotted with respect to $\log(t_9)$. The four points about $\log(t_9) = 0.47$ are for the mass−gaining EBs. These binaries are not included in fitting the line for the age−metallicity relation. The minimum value of Z is assumed to be zero at $t_9 = 13.4$.

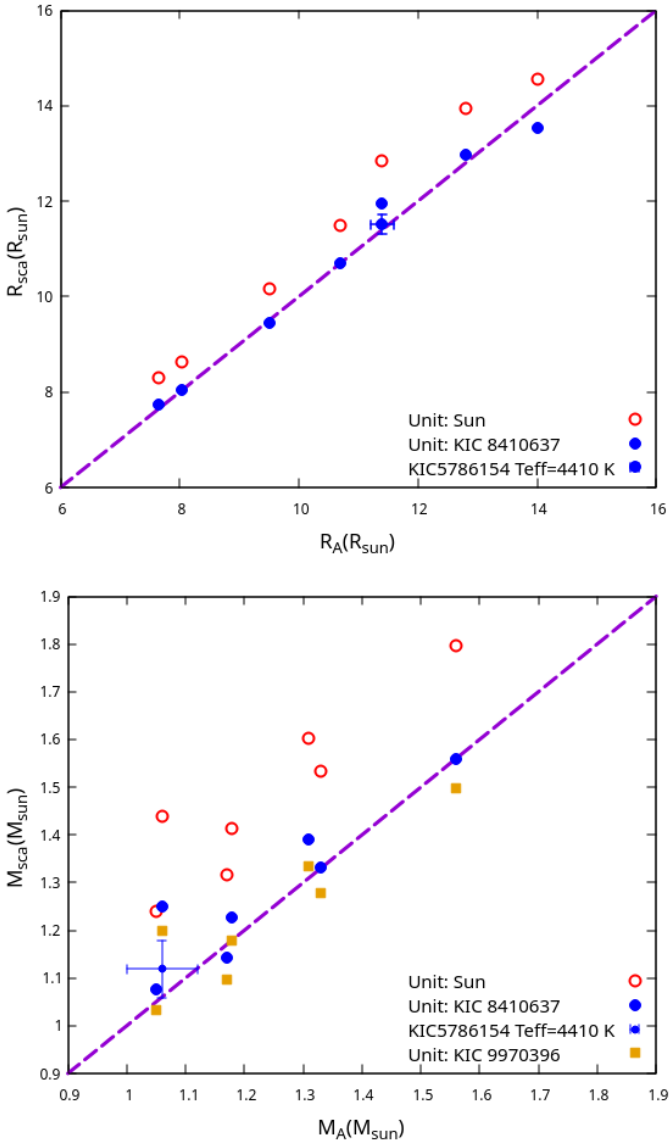

Figure 10. $R_{\rm sca}$, computed using KIC8410637 as a unit star for the asteroseismic scaling relations, is plotted against the observed radius (filled circles). For comparison, $R_{\rm sca}$ computed from the solar values (circles) are also plotted. The lower panel shows $M_{\rm sca}$. KIC 9970396 is also used as a unit star (squares).

4.7.1 Role of the unit stars in the scaling relations

There are serious differences between M and R obtained from the dynamical data of these EBs and $M_{\rm sca}$ and $R_{\rm sca}$ obtained from the scaling relations (Eqs. 1). Based on these differences, we can determine the type of corrections required. Many studies explored this subject (Huber et al. 2017; Li et al. 2022; Yıldız 2023). In this study, for the first time, instead of the Sun as the unit star, we calculated $M_{\rm sca}$ and $R_{\rm sca}$ using one of the stars, such as KIC 8410637 A, for which there was sufficiently good agreement between the model and observation. In Fig. 10a, we plot the $R_{\rm sca}$ calculated using KIC 8410637 A as the unit star against $R_{\rm A}$ for the primary stars. For comparison, the $R_{\rm sca}$ values using the Sun as the unit star are also shown. The agreement between $R_{\rm sca}$ and $R_{\rm A}$ demonstrates that using KIC 8410637 A as the unit star gives much better results than those obtained using the Sun as the unit star. We also compute the $R_{\rm sca}$ of the primary stars using KIC 9970396 A as a unit star. We obtain exactly the same results as those obtained for KIC 8410637 A.

In the lower panel of Fig. 10, $M_{\rm sca}$ is plotted against $M_{\rm A}$. There is a large difference between $M_{\rm sca}$ and $M_{\rm A}$ when we use the uncorrected scaling relations (Eq. 1) with the Sun as a unit star. Compared to the Sun, the unit stars KIC 8410637 A and KIC 9970396 A provide much more compatible results for the mass. In particular, KIC 8410637 A as a unit star provides more compatible results for $M_{\rm sca}$ and $M_{\rm A}$.

A comparison of the dynamical and asteroseismic M and R reveals a clear difference, especially in the case of KIC 5786154. These differences may be due to $T_{\rm eff}$. Gaulme et al. (2016) reported the highest $T_{\rm eff}$ (4747 K). From their work, the $T_{\rm eff}$ required for the fit can be found. The points shown with error bars indicate the result obtained with $T_{\rm eff} = 4410$ K for this star.

Table 6. Modelled and observed frequencies for Tek Ayak. The columns give the l degree of the modes, model frequencies obtained by Methods I and II and the observed frequencies (ν_{obs}). The values of ν_{max} and $\Delta\nu$ are given at the end of the table. The last row gives the observational $\Delta\nu$ value calculated from the $\Delta\nu-\nu$ graph.

l	Method I ν (μHz)	Method II ν (μHz)	ν_{obs} (μHz)
0	32.8522	32.8018	32.79±0.02
0	37.1843	37.1533	37.18±0.02
0	41.5944	41.6178	41.62±0.01
0	46.2740	46.2774	46.28±0.02
0	50.8287	50.8363	50.85±0.01
0	55.5219	55.5359	55.54±0.03
0	60.2934	60.2756	60.28±0.05
1	35.1028	35.4505	35.16±0.04
1	39.4455	39.3699	39.44±0.02
1	44.0731	44.0478	44.06±0.02
1	48.9994	48.9702	48.70±0.02
1	53.7799	52.9729	53.32±0.02
1	58.4260	57.9178	58.04±0.04
1	63.9828	62.9079	62.95±0.02
2	31.1358	32.1580	32.13±0.05
2	36.5416	36.5017	36.56±0.03
2	41.0207	41.0565	41.02±0.01
2	45.6303	45.5811	45.69±0.01
2	50.2423	50.4990	50.31±0.02
2	54.9907	55.1014	55.06±0.04
2	60.4569	60.0054	59.74±0.05
3	37.7642	37.7136	37.70±0.09
3	47.3715	47.0210	47.19±0.01
3	51.0233	51.7589	51.71±0.06
ν_{max} (μHz)	46.5033	46.2160	46.00±0.19
$\Delta\nu$ (μHz)	4.5735	4.5790	4.641±0.017
$\Delta\nu$ (μHz)	——	——	4.5817±0.0577

4.7.2 *Comparison of the model and observed individual frequencies of Tek Ayak*

Among the RGs we analysed, Tek Ayak is one of the two stars with observed frequencies. Interior models are constructed with MESA astero module to compare the observed and model frequencies of Tek Ayak, which is taken as the unit star. The astero module uses two different inlists. The inlist from the star package is used in `inlist_example_astero`, while `inlisti_astero_search_controls` contains asteroseismic and non-asteroseismic parameters determined from observations such as T_{eff}, R, [M/H], $\Delta\nu$, ν_{max} and ν. The ADIPLS package is used for the frequency calculations. The 'combined' option of Ball & Gizon (2014) is used to calculate near-surface effects at different frequencies.

In the astero module, interior models are constructed using the model results given in Table 3 for Methods I and II. The obtained adiabatic oscillation frequencies are listed in Table 6. The following results are obtained using Method I: $\Delta\nu$ = 4.5735 μHz, ν_{max} = 46.5033 μHz, T_{eff} = 4800.8 K, R = 10.68 $R_\odot$ and t_9 = 2.167 Gyr. The results obtained using Method II are as follows: $\Delta\nu$ = 4.5790 μHz, ν_{max} = 46.2160 μHz, T_{eff} = 4799.5 K, R = 10.71 $R_\odot$ and t_9 = 2.303 Gyr. The values of $\Delta\nu$ are calculated from the $\Delta\nu-\nu$ graph for the l = 0 mode frequencies. Calculation of the observed $\Delta\nu$ value by this method yielded the value 4.5817±0.0577 μHz. The modelled $\Delta\nu$s values agree well with this value. The observed ν_{max} shows better agreement with the value obtained by Method II.

The difference between the observed and model frequencies is less than 1% for Method I and Method II. For Method I, the mean fractional differences at mode frequencies l = 0, 1, 2 and 3 are 0.0001, 0.0030, 0.0011 and 0.0039, respectively. For Method II, the mean fractional differences are -0.0001, 0.0004, 0.0010 and -0.0008, respectively. Although the frequencies are compatible with each other, the patterns on the $\Delta\nu-\nu$ graph may differ. Although the frequency patterns of both models are compatible in the $\Delta\nu-\nu$ graph drawn from l = 0 frequencies, Method II is much more compatible with the observation.

Another star whose observation frequencies have been determined is KIC 9540226. Although the results are not as good as those of Tek Ayak, interior models are constructed for this star with the astero module. The mean fractional differences between the model and observation frequencies for l = 0, 1 and 2 are 0.0003, -0.0008, and 0.0037, respectively, for Method I and 0.0001, -0.0011 and 0.0024, respectively, for Method II. The $\Delta\nu$ values determined from the frequencies of the modes with l = 0 for Methods I and II are 3.165 and 3.169 μHz, respectively ($\Delta\nu_{obs}$ = 3.194 μHz with this method). The $\Delta\nu$ value of both models and the patterns in the $\Delta\nu-\nu$ graph are less consistent with the observations than those of Tek Ayak. The ν_{max} values are 28.09 and 27.60 μHz.

5 CONCLUSIONS

In this study, we comprehensively analysed 11 double-lined EBs with SLOs by using two distinct methods to determine the ages and chemical compositions of their components. Our findings provide valuable insights into the evolutionary processes, mass transfer mechanisms and asteroseismic properties of these systems.

Key Findings:

1. Mass Transfer and Evolution:

We identified several candidate systems for mass transfer, including KIC 4054905, KIC 10001167, KIC 8430105 and KIC 9540226. These systems exhibit clear evidence of mass loss or gain, as inferred from their positions in the MZ diagram. For instance, the primary component of KIC 4054905 has less mass and a larger radius than its secondary component, strongly indicating mass transfer. Similarly, KIC 10001167 and KIC 8430105 are located outside the MZ triangle, suggesting a significant mass loss or gain.

The mass transfer processes in these systems are further supported by the discrepancies in the ages of their components when modelled under the assumption of constant mass. For example, KIC 10001167 exhibits an unrealistic age of 19.81 Gyr when modelled with constant mass, implying that mass loss must have occurred if the observed properties are to be attained.

2. Chemical Evolution:

Our analysis of Y_0 and Z_0 reveals a clear relationship of these parameters with the ages of the systems. The Y_0 values obtained by Methods I and II are consistent with the Y_p of the galaxy, in agreement with the chemical enrichment law $Y = Y_p + 2Z$. The metallicity−age relationship further confirms the chemical evolution of these systems, with older systems generally exhibiting lower metallicities, as expected from the galactic chemical evolution models.

3. Asteroseismic Properties:

The asteroseismic analysis of the primary components of the EBs shows good agreement between the observed and modelled values of $\Delta\nu$ and ν_{max}. This agreement validates the use of asteroseismic scaling relations to determine the stellar properties.

We also demonstrated the utility of using specific SLO stars (e.g. KIC 8410637 and KIC 9970396) as unit stars in asteroseismic scaling relations, thereby significantly improving the accuracy of the derived masses and radii compared to those obtained using the Sun as a reference.

4. Methodological Insights:

Method I (varying Y_0): This method provided ages in the range of 2.17−5.79 Gyr, with Y_0 values of 0.2381−0.3039. However, for some systems, such as KIC 4054905 and KIC 10001167, the solutions are either unattainable or require extreme values of Y_0, highlighting the limitations of this approach in the case of significant mass transfer.

Method II (varying Z_0): This method yielded more consistent results, with ages of 2.30−6.13 Gyr and Y_0 values of 0.2545−0.2797. The narrower range of Y_0 and better agreement with observational constraints suggest that Method II is more robust, particularly for systems with complex evolutionary histories.

Implications and Future Work:

Our results underscore the importance of considering mass transfer and chemical evolution when modeling binary systems. The discrepancies between the observed and modelled properties of some systems (e.g., KIC

10001167) highlight the need for more sophisticated models that account for the mass loss and accretion processes. Future studies should focus on developing such models, incorporating detailed treatments of the mass transfer and its impact on the chemical and structural evolution of the binary components.

Additionally, the use of SLO stars as unit stars in asteroseismic scaling relations opens new avenues for improving the accuracy of asteroseismic analyses. Further investigations into the calibration of these relations using a larger sample of well-characterised SLO stars can significantly enhance our ability to precisely determine stellar properties.

In conclusion, this study provides a detailed understanding of the evolutionary and asteroseismic properties of the SLO RGs in EBs, shedding light on the complex interplay between mass transfer, chemical evolution and stellar structure in binary systems. Our findings pave the way for future research aimed at refining stellar models and scaling relations, ultimately contributing to a deeper understanding of stellar astrophysics.

ACKNOWLEDGEMENTS

This study was supported by Scientific and Technological Research Council of Turkey (TÜBITAK) under the Grant Number 123F019. We are grateful to Ege University Planning and Monitoring Coordination of Organizational Development and Directorate of Library and Documentation for their support in the editing and proofreading service of this study.

DATA AVAILABILITY

The data underlying this article will be shared on reasonable request to the corresponding author.

REFERENCES

Ball W. H., Gizon L., 2014, A&A, 568, A123. doi:10.1051/0004-6361/201424325
Beck P. G., Hambleton K., Vos J., Kallinger T., Bloemen S., Tkachenko A., García R. A., et al., 2014, A&A, 564, A36. doi:10.1051/0004-6361/201322477
Beck P. G., Grossmann D. H., Steinwender L., Schimak L. S., Muntean N., Vrard M., Patton R. A., et al., 2024, A&A, 682, A7. doi:10.1051/0004-6361/202346810
Benbakoura M., Gaulme P., McKeever J., Sekaran S., Beck P. G., Spada F., Jackiewicz J., et al., 2021, A&A, 648, A113. doi:10.1051/0004-6361/202037783
Böhm-Vitense E., 1958, Zeitschrift für Astrophysik, 46, 108
Borucki W. J., Koch D., Basri G., Batalha, N., Broen, T., et al. 2010, Science, 327, 977
Brogaard K., Jessen-Hansen J., Handberg R., Arentoft T., Frandsen S., Grundahl F., Bruntt H., et al., 2016, AN, 337, 793. doi:10.1002/asna.201612374
Brogaard K., Hansen C. J., Miglio A., Slumstrup D., Frandsen S., Jessen-Hansen J., Lund M. N., et al., 2018, MNRAS, 476, 3729. doi:10.1093/mnras/sty268
Brogaard K., Arentoft T., Slumstrup D., Grundahl F., Lund M. N., Arndt L., Grund S., et al., 2022, A&A, 668, A82. doi:10.1051/0004-6361/202244345
Brown, T.M., Gilliland R.L., Noyes, R.W., Ramsey, L.W., 1991, ApJ, 368, 599
Brown T. M., Latham D. W., Everett M. E., Esquerdo G. A., 2011, AJ, 142, 112. doi:10.1088/0004-6256/142/4/112
Christensen-Dalsgaard J., 1993, ASPC, 42, 347
Ferguson, J.W., Alexander, D.R., Allard, F., Barmanu, T., et al. 2005, ApJ, 623, 585
Frandsen S., Lehmann H., Hekker S., Southworth J., Debosscher J., Beck P., Hartmann M., et al., 2013, A&A, 556, A138. doi:10.1051/0004-6361/201321817
Gaia Collaboration, Brown A. G. A., Vallenari, A., Prusti, T., de Bruijne, J.H.J., et al., 2018, A&A, 616, A1
Gaia Collaboration, Brown A. G. A., Vallenari, A., Prusti, T., de Bruijne, J.H.J., et al., 2021, A&A, 649, A1
Gaulme P., McKeever J., Jackiewicz J., Rawls M. L., Corsaro E., Mosser B., Southworth J., et al., 2016, ApJ, 832, 121. doi:10.3847/0004-637X/832/2/121
Gaulme P., Jackiewicz J., Spada F., Chojnowski D., Mosser B., McKeever J., Hedlund A., et al., 2020, A&A, 639, A63. doi:10.1051/0004-6361/202037781
Gaulme P., Borkovits T., Appourchaux T., Pavlovski K., Spada F., Gehan C., Ong J., et al., 2022, A&A, 668, A173. doi:10.1051/0004-6361/202244373
Gratton R. G., Bragaglia A., Carretta E., Clementini G., Desidera S., Grundahl F., Lucatello S., 2003, A&A, 408, 529. doi:10.1051/0004-6361:20031003
Grossmann D. H., Beck P. G., Mathur S., Johnston C., Godoy-Rivera D., Zinn J. C., Cassisi S., et al., 2025, arXiv, arXiv:2501.09018. doi:10.48550/arXiv.2501.09018
Hekker S., Debosscher J., Huber D., Hidas M. G., De Ridder J., Aerts C., Stello D., et al., 2010, ApJL, 713, L187. doi:10.1088/2041-8205/713/2/L187
Huber D., Zinn J., Bojsen-Hansen M., Pinsonneault M., Sahlholdt C., Serenelli A., Silva Aguirre V., et al., 2017, ApJ, 844, 102. doi:10.3847/1538-4357/aa75ca
Iglesias C. A., Rogers F. J., 1993, ApJ, 412, 752. doi:10.1086/172958
Iglesias C.A., and Rogers F.J. 1996, ApJ, 464, 943
Jermyn A. S., Bauer E. B., Schwab J., Farmer R., Ball W. H., Bellinger E. P., Dotter A., et al., 2023, ApJS, 265, 15. doi:10.3847/1538-4365/acae8d
Kjeldsen H., and Bedding T. R. 1995, A&A, 293, 87
Li T., Li Y., Bi S., Bedding T. R., Davies G., Du M., 2022, ApJ, 927, 167. doi:10.3847/1538-4357/ac4fbf
Paquette C., Pelletier C., Fontaine G., Michaud G., 1986, ApJS, 61, 177. doi:10.1086/191111
Paxton B., Bildsten L., Dotter A., Herwig F., Lesaffre P. and Timmes F., 2011, ApJS, 192, 35
Paxton B., Cantiello M., Arras P., Bildsten L., Brown, E.F, et al., 2013, ApJS, 208, 42
Paxton B., Marchant P., Schwab J., Bauer E. B., Bildsten L., Cantiello M., Dessart L., et al., 2015, ApJS, 220, 15. doi:10.1088/0067-0049/220/1/15
Paxton B., Schwab J., Bauer E. B., Bildsten L., Blinnikov S., Duffell P., Farmer R., et al., 2018, ApJS, 234, 34. doi:10.3847/1538-4365/aaa5a8
Paxton B., Smolec R., Schwab J., Gautschy A., Bildsten L., Cantiello M., Dotter A., et al., 2019, ApJS, 243, 10. doi:10.3847/1538-4365/ab2241
Pinsonneault M. H., Elsworth Y. P., Tayar J., Serenelli A., Stello D., Zinn J., Mathur S., et al., 2018, ApJS, 239, 32. doi:10.3847/1538-4365/aaebfd
Planck Collaboration, Aghanim N., Akrami Y., Ashdown M., Aumont J., Baccigalupi C., Ballardini M., et al., 2020, A&A, 641, A6. doi:10.1051/0004-6361/201833910
Rawls M. L., Gaulme P., McKeever J., Jackiewicz J., Orosz J. A., Corsaro E., Beck P. G., et al., 2016, ApJ, 818, 108. doi:10.3847/0004-637X/818/2/108
Rowan D. M., Stanek K. Z., Kochanek C. S., Thompson T. A., Jayasinghe T., Blaum J., Fulton B. J., et al., 2024, arXiv, arXiv:2409.02983. doi:10.48550/arXiv.2409.02983
Sharma S., Stello D., Bland-Hawthorn J. et al. 2016, ApJ, 822, 15
Skrutskie M. F., Cutri R. M., Stiening R., Weinberg M. D., Schneider S., Carpenter J. M., Beichman C., et al., 2006, AJ, 131, 1163. doi:10.1086/498708
Sullivan, P. W., Winn, J.N., Berta-Thompson, Z.K., Charbonneau, D., Deming, D., et al., 2015, ApJ, 809, 77
Tassoul M., 1980, ApJS, 43, 469. doi:10.1086/190678
Themeßl N., Hekker S., Southworth J., Beck P. G., Pavlovski K., Tkachenko A., Angelou G. C., et al., 2018, MNRAS, 478, 4669. doi:10.1093/mnras/sty1113
Wenger M., Ochsenbein F., Egret D., Dubois P., Bonnarel F., Borde S., Genova F., et al., 2000, A&AS, 143, 9. doi:10.1051/aas:2000332
Yıldız M., Doğan T., 2013, MNRAS, 430, 2029. doi:10.1093/mnras/stt028
Yıldız M., Örtel S., 2021, MNRAS, 504, 2273. doi:10.1093/mnras/stab996
Yıldız M., 2023, MNRAS, 518, 5552. doi:10.1093/mnras/stac3464

This paper has been typeset from a TEX/LATEX file prepared by the author.